For publication in Ships and Offshore Structures

Fire hazard identification on the flight deck of a short-take-off/vertical-landing type aircraft carrier: Fire scenarios selection

Jeong Hwan Kim[a], Seon Jin Kim[b], Dae Yu Baeg[b], Hyun Ho Lee[b], Jung Kwan Seo[a,b*], Jeom Kee Paik[a,c]

[a]The Korea Ship and Offshore Research Institute (Lloyd's Register Foundation Research Centre of Excellence), Pusan National University, Busan, Republic of Korea

[b]Department of Naval Architecture and Ocean Engineering, Pusan National University, Busan, Republic of Korea

[c] Department of Mechanical Engineering, University College London, London, UK

[*] Corresponding author. Tel.: +82 51 510-2415. *Email address:* seojk*@pusan.ac.kr* (J.K. Seo).

Abstract: The flight deck of aircraft carriers in operation is exposed to fire risks which must be mitigated by fire safety measures such as firefighting and suppression systems. To develop advanced fire safety measures, the quantitative risk assessment and management is essential, where fire hazards must be identified in a probabilistic manner considering operational conditions (e.g., sortie generation rates) and site-specific ocean environmental conditions (e.g., humidity, wave and wind profiles). In this paper, a set of realistic fire scenarios on the flight deck of a hypothetical short take-off/vertical landing (STOVL) type aircraft carrier are selected, which shall be used for the quantitative fire risk assessment and management. Potential fire hazards are formulated as a function of random parameters associated with operational and ocean environmental conditions, and probabilistic sampling technique is used to select hundred fire scenarios. Fire exceedance diagrams are established in association with fire-impacted (leak) area through the selected fire scenarios.

Keywords: Aircraft carrier, flight deck, short take-off/vertical landing (STOVL), fire hazard identification, quantitative fire risk assessment and management

1. Introduction

The flight deck of an aircraft carrier must exhibit high survivability to ensure its active defence capability. Fire hazards on the flight deck of aircraft carriers are owing to four main sources: presence of large quantities of fuel and a wide variety of ordnance, rapid/close proximity operations, and ocean environments. Specifically, fuelled aircrafts carry large quantities of fuel and perform frequent fuelling and de-fuelling operations. Air-launched ordnance with various types (e.g., missiles, bombs, and guns) is placed on or near the flight deck. Aircraft movement and rearrangement can be frequent on the flight deck, depending on the landing and take-off requirements, and numerous supporting vehicles and human traffic can also be present. Such deck operations are performed rapidly and close to critical areas, resulting in volatile situations. In addition, the ocean environment, which involves wind and wave action, may influence the flame spread characteristics.

A typical flight deck of aircraft carriers has a variety of ignition sources such as hot engines, exhaust from aircraft engines and supporting vehicles, and aviation support equipment. Other sources of fires and explosions may include in-service conditions such as electrical arcing, sparking potential, hot works (e.g., flame cutting and welding), static discharges, electromagnetic radiation, catapult steam lines, aircraft crashes, ordnance firing, and arson/terrorism. Enemy action in combat may also lead to the introduction of various ignition sources (Darwin et al. 2005).

Figure 1. Fire accidents on the flight deck of Nimitz (CVN-68) (left) and Forrestal (CV-59) (right).

Most accidents that occur on aircraft carriers are attributable to aviation fuel (Lee 2021), weapons, and aircraft collisions and involve blast effects and heat. Such accidents lead to critical consequences in terms of human health, structural safety, and safety of the surrounding

environment (Nolan 1996; Darwin et al. 2002; Paik 2020, 2022). Fire and explosion events arising from aircraft collisions (e.g., on CVN-68, see the left photo of Figure 1) and malfunctioning of air weapons (on CV-59, see the right photo of Figure 1), can cause considerable damage to carriers and their crew.

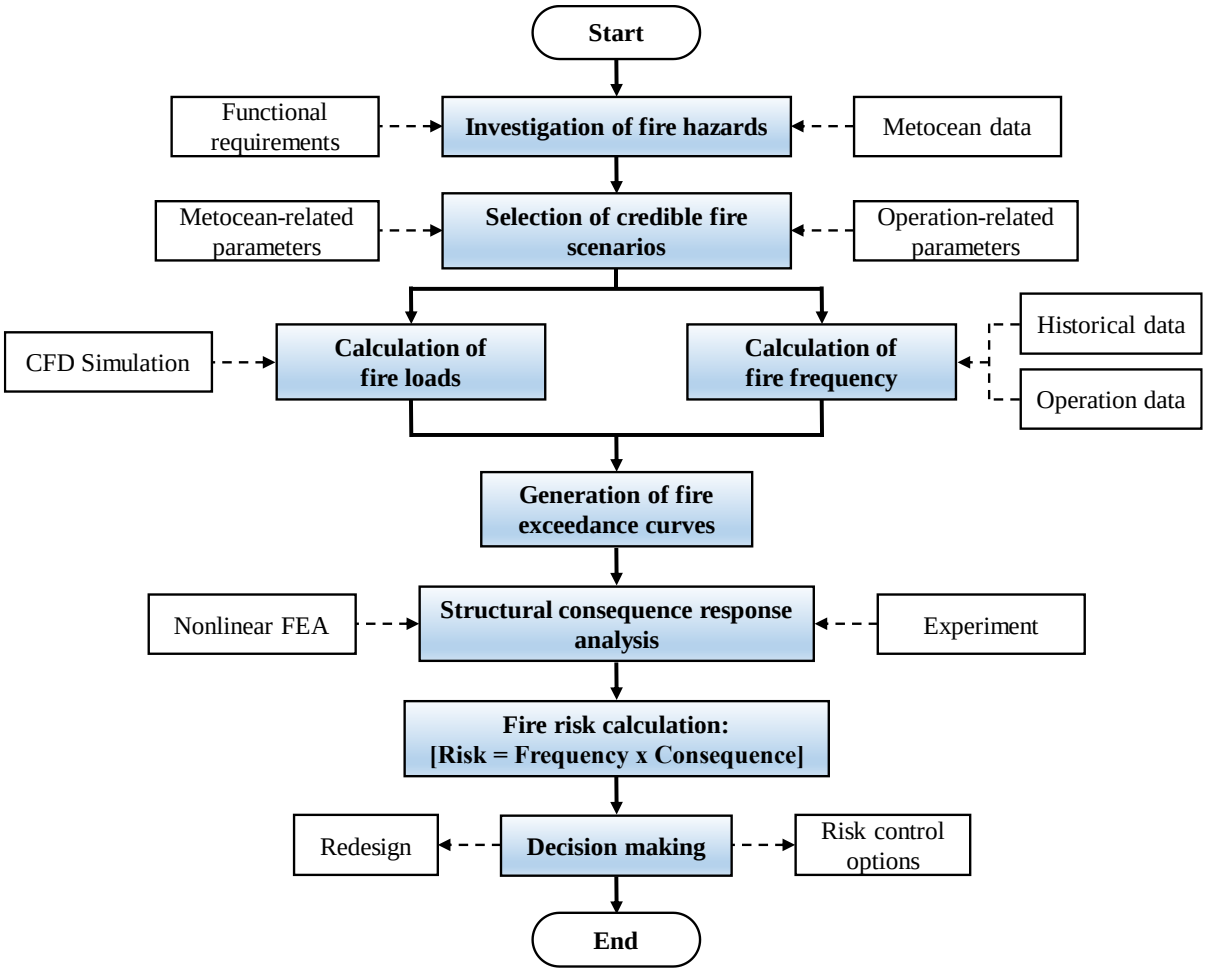

Figure 2. Procedure for the quantitative fire risk assessment and management, originally proposed by Paik (2020).

To develop advanced safety measures for preventing the escalation of such events, detailed knowledge of the related phenomena and their consequences are essential. Concerns regarding fire and explosion risks are reflected in the industry rules and schemes for quantitative risk assessment and management, which typically require firefighting systems to attain high recoverability (DNV 2015; IMO 2015). In the wake of fire disasters in naval ships, damage control and firefighting (DCFF) exercises have been established, and new aircraft design and assessment strategies have been formulated to examine vulnerability and ensure recoverability.

In engineering community, risk is defined as a product of the frequency of an accident and its consequence (Paik 2020, 2022). Within the framework of quantitative risk assessment and management for an accident, a set of realistic accident scenarios should be selected unlike deterministic approaches in that the 'most unfavourable scenario' is considered. For this purpose, Paik (2020) originally proposed an accurate and efficient method to select a set of realistic accident scenarios within the framework of quantitative risk assessment and management, see Figures 2 and 3. In this paper, the Paik method is used to identify fire hazards and select the fire scenarios on the flight deck of an aircraft carrier, where the specific details of the process are shown in Figure 4. The flight deck of a hypothetical short take-off/vertical landing (STOVL) type aircraft carrier is considered, similar to that of the Queen Elizabeth (QE) class aircraft carrier and/or America-class carriers. The flight deck has two islands and lift locations, similar to the QE class aircraft carrier, as shown in Figure 5 (BAE 2022).

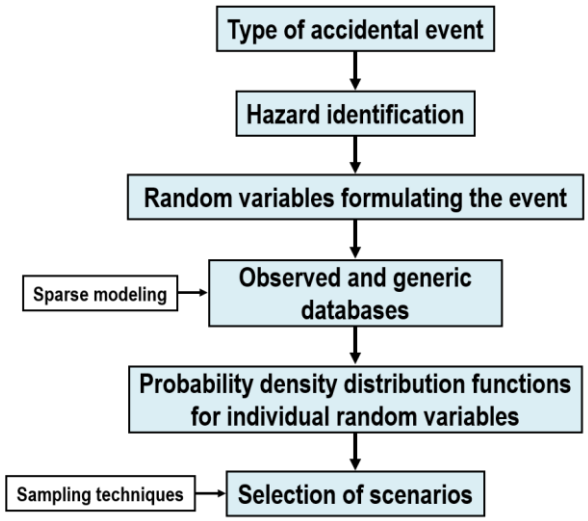

Figure 3. A general procedure for probabilistic selection of accident scenarios, originally proposed by Paik (2020).

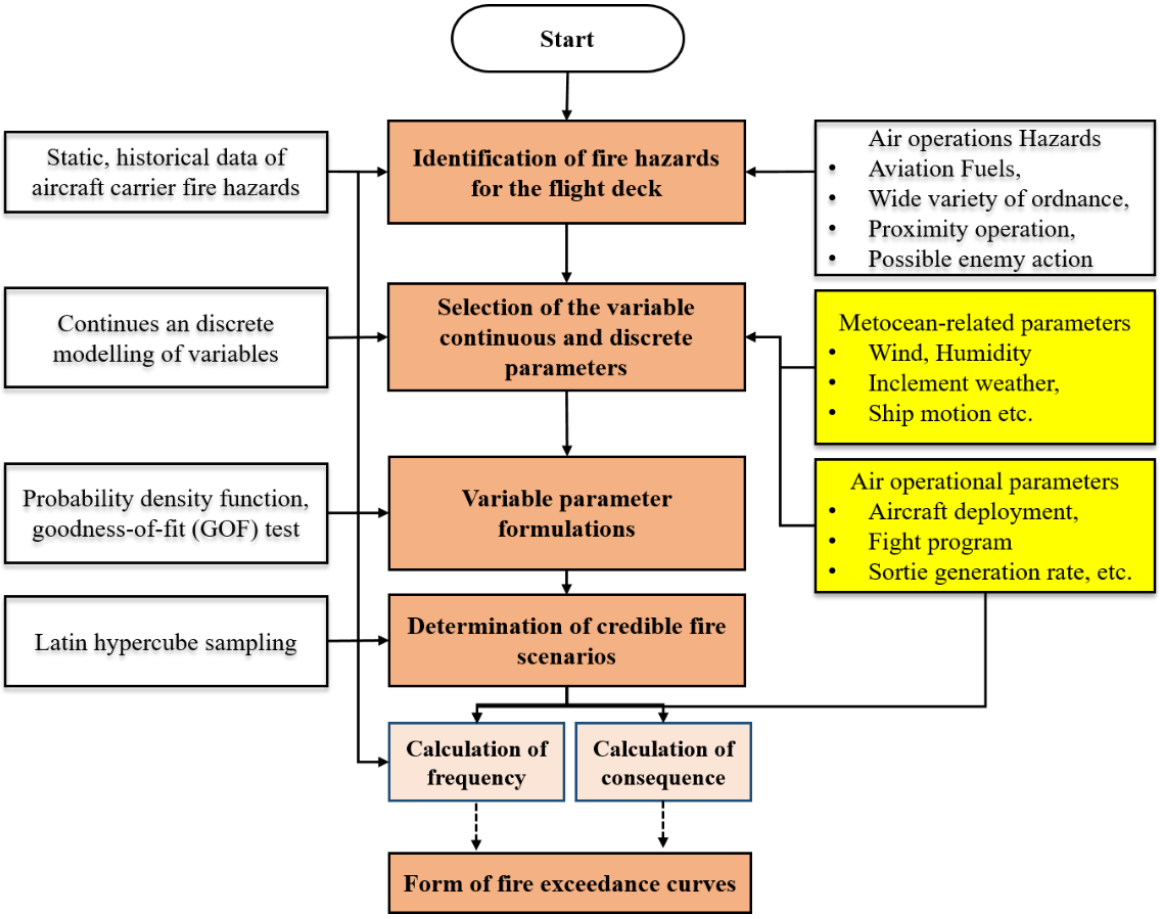

Figure 4. Details of the process to select fire scenarios on the flight deck of aircraft carriers, applied in the present paper.

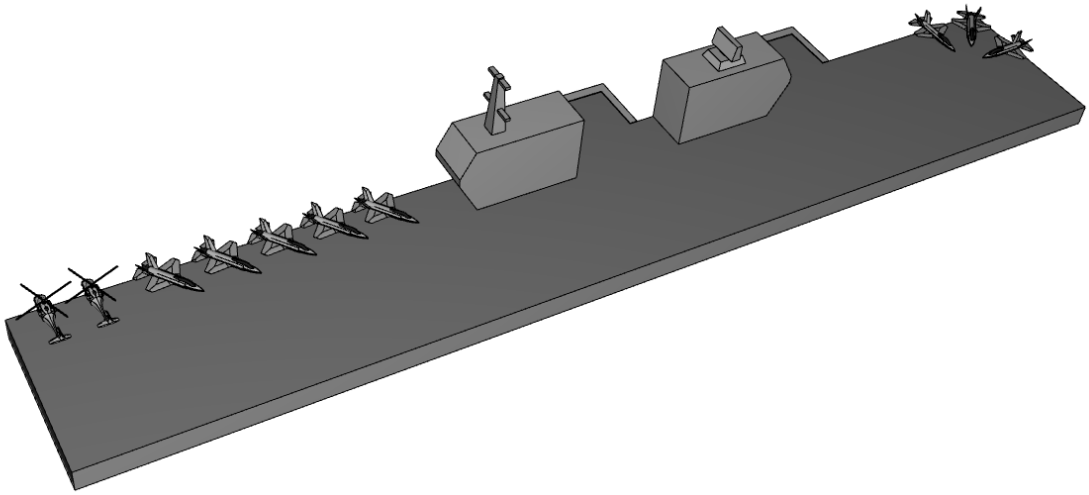

Figure 5. A schematic of the flight deck of a QE class STOVL type aircraft carrier (BAE 2022).

2. Fire hazard identification and random parameters

Fire hazard identification is made based on the historical database which are available in the literature. Leonard et al. (1992) surveyed the historical data of fire accidents on the flight deck of aircraft carriers. A representative example of a fire accident is one that occurred on the flight deck of Nimitz (CVN-68) in 1981: An aircraft attempting to land drifted to the right of the flight deck centreline and struck the tail of a helicopter, three parked aircraft, a tow tractor, and three F-14 aircraft before coming to rest on the port edge of the flight deck. An intense fuel fire erupted on the flight deck, leading to the combustion of the energetic fillers in the ordnance and pyrotechnics(Seaforces: www.seaforces.org). Aircraft crashes that produced large pool fires and three-dimensional fires (Kim et al. 2016; Chung et al. 2021) and fires threatening ordnance have proven to have the worst outcomes.

The variables associated with the sources of fire hazards on the flight deck of aircraft carriers can be categorized in association with the large quantities of fuel, the wide variety of ordnance, rapid/close proximity operations, and the ocean environment. Specifically, fuelled aircrafts carry large quantities of fuel, and fuelling and de-fuelling operations are frequent. Air-launched ordnance of various types (missiles, bombs, and guns) is placed on or near the flight deck. Aircraft movement and rearrangement can be frequent on the flight deck, depending on the landing and take-off requirements, and numerous supporting vehicles and human traffic can also be present. Such deck operations are often performed rapidly and close to critical areas, resulting in volatile situations. Therefore, the variables associated with the aforementioned first three categories of sources must be characterised to represent the air operations in the vicinity of the flight deck and the specified flight programme of the sortie generation rates (SGR) to meet the mission of the aircraft carrier. In the preparation of take-offs on the flight deck, fore hazards are significantly affected by wind conditions (e.g., wind direction and velocity) and aircraft arrangement (e.g., ignition location and amount of fuel in the flight tanks).

The ocean environment influences the fire consequences such as the flame spreading characteristics. The variables representing the environmental conditions are characterised from observed data on the flight deck and general knowledge regarding the potential operational areas of the carrier. Ocean environmental data such as wave, wind, humidity, and air temperature are primary parameters that affect fire accidents.

In this regard, a total of seven random variables (parameters) are considered to represent fire hazards on the flight deck of aircraft carriers.

- Wind direction (X_1)

- Wind speed (X_2)
- Humidity (X_3)
- Oil or gas leak location (X_4)
- Oil or gas leak amount (X_5)
- Ship roll angle (X_6)
- Ship pitch angle (X_7)

Strictly speaking, variables X_6 and X_7 are associated with ship motions which are governed by ship operational conditions (e.g., ship speed) and ocean wave profiles (e.g., wave height, wave duration and heading angle) together with the site-specific metocean data at the operating water (e.g., in Korean seas). Ship motions can be simulated by computational fluid dynamics (CFD) methods, but for the purpose of simplicity, the present study defines them by representative parameters of ship motions in terms of roll and pitch associated with the operational capacity of the target ship.

3. Probabilistic characterization of random variables

Each of random variables is characterized by a probability density distribution function (PDF) which is based on the historical data and site-specific metocean data. The range of each variable is defined in association with the discrete or continuous environmental conditions. In major accidents or high-risk scenarios, all random variables are likely to be correlated. For example, the leak amount of fuel (kg), expressed as a product of the leak duration (s) and leak rate (kg/s) is associated with geometric and environmental factors as well as ignition location. Therefore, these variables are formulated as independent variables within their potential ranges.

With historical accident data as well as operational and ocean environmental data, the probability density distribution of each variable can be characterized by a histogram with the corresponding range and variability. The histogram is then formulated by a continuous function (PDF) through the goodness-of-fit (GOF) test, which best represents the database.

3.1 Wind direction (X_1) and speed (X_2)

The probabilistic characteristics of wind speed and direction can be determined from metocean (wind rose) data at the operating site of the aircraft carrier. Unlike offshore platforms that operate only in a specific location, aircraft carriers may operate in a specific region or

worldwide. Therefore, these variables are characterised with metocean data of specific and/or possible operation regions.

In this study, the ocean environmental data collected for 10 years around the Korean peninsula was used to create the corresponding histograms. The bin width of the variable to establish the histogram was 30° for wind direction and 1 m/s for wind speed. The average values of wind direction and speed are summarised in Table 1.

Table 1. Metocean data for wind direction and speed around the considered ocean region (Korean peninsula)

		Average wind speed (m/s)																							
		0–1	1–2	2–3	3–4	4–5	5–6	6–7	7–8	8–9	9–10	10–11	11–12	12–13	13–14	14–15	15–16	16–17	17–18	18–19	19–20	20–21	21–22	22–23	Total
Average wind direction (°)	0–30	0.15	0.66	1.02	1.27	1.39	1.48	1.42	1.38	1.34	1.18	0.96	0.71	0.44	0.25	0.13	0.05	0.02	0.01	0.00	0.00	0.00	0.00	0.00	**13.89**
	30–60	0.25	0.63	0.87	0.98	0.92	0.84	0.77	0.67	0.51	0.40	0.29	0.17	0.12	0.06	0.03	0.01	0.01	0.00	0.00	0.00	0.00	0.00	0.00	**7.53**
	60–90	0.26	0.60	0.75	0.75	0.70	0.59	0.54	0.47	0.39	0.28	0.22	0.15	0.10	0.05	0.03	0.02	0.01	0.01	0.00	0.00	0.00	0.00	0.00	**5.92**
	90–120	0.29	0.62	0.82	0.79	0.78	0.73	0.68	0.62	0.51	0.39	0.26	0.16	0.14	0.08	0.05	0.02	0.01	0.01	0.00	0.00	0.00	0.00	0.00	**6.95**
	120–150	0.24	0.65	0.97	1.08	0.92	0.78	0.58	0.41	0.26	0.15	0.08	0.05	0.03	0.02	0.02	0.00	0.01	0.00	0.00	0.00	0.00	0.00	0.00	**6.26**
	150–180	0.26	0.62	1.03	1.28	1.32	1.18	0.95	0.71	0.39	0.22	0.13	0.08	0.04	0.02	0.01	0.01	0.00	0.00	0.00	0.00	0.00	0.00	0.00	**8.27**
	180–210	0.25	0.62	0.96	1.19	1.31	1.31	1.15	1.03	0.78	0.50	0.29	0.17	0.09	0.05	0.02	0.01	0.01	0.00	0.00	0.00	0.00	0.00	0.00	**9.75**
	210–240	0.25	0.61	0.85	0.93	0.87	0.78	0.64	0.51	0.36	0.24	0.14	0.08	0.04	0.02	0.01	0.00	0.00	0.00	0.00	0.00	0.00	0.00	0.00	**6.33**
	240–270	0.24	0.59	0.73	0.70	0.62	0.50	0.40	0.31	0.20	0.14	0.10	0.05	0.02	0.02	0.01	0.00	0.00	0.00	0.00	0.00	0.00	0.00	0.00	**4.63**
	270–300	0.25	0.57	0.71	0.72	0.69	0.58	0.55	0.48	0.40	0.32	0.25	0.17	0.12	0.08	0.05	0.02	0.01	0.00	0.00	0.00	0.00	0.00	0.00	**5.96**
	300–330	0.25	0.58	0.82	0.93	0.95	0.93	0.88	0.87	0.83	0.71	0.58	0.45	0.33	0.22	0.13	0.05	0.02	0.01	0.00	0.00	0.00	0.00	0.00	**9.55**
	330–360	0.25	0.64	0.97	1.18	1.32	1.37	1.46	1.37	1.33	1.26	1.14	0.92	0.70	0.44	0.24	0.09	0.03	0.01	0.00	0.00	0.00	0.00	0.00	**14.73**
	Total	**3.15**	**7.39**	**10.49**	**11.81**	**11.80**	**11.09**	**10.01**	**8.81**	**7.28**	**5.79**	**4.44**	**3.17**	**2.18**	**1.31**	**0.73**	**0.30**	**0.13**	**0.05**	**0.02**	**0.01**	**0.01**	**0.00**	**0.01**	**100.00**

Table 2(a). Probability density of wind direction for the considered ocean area

Wind direction (°)	Probability density
0–30	0.00463
30–60	0.00251
60–90	0.00198
90–120	0.00232
120–150	0.00209
150–180	0.00276
180–210	0.00325
210–240	0.00211
240–270	0.00154
270–300	0.00199
300–330	0.00318
330–360	0.00491

Table. 2(b). Probability density of wind speed for the considered ocean area

Wind speed (m/s)	Probability density
0–3	0.0701
3–6	0.1157
6–9	0.0870
9–12	0.0447
12–15	0.0141
15–18	0.0016
18–21	0.0001
21–24	4.6484E-05
24–27	9.0385E-06
27–30	4.0385E-07

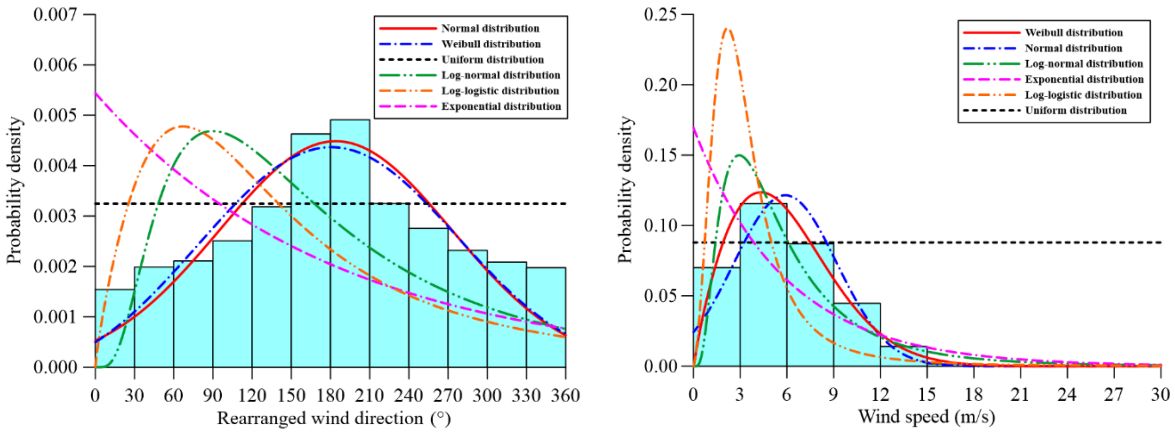

(a) Wind direction (b) Wind speed

Figure 6. Probability density functions (PDFs) for (a) wind direction (*X1*) and (b) wind speed (*X2*).

Table 2 presents the probability densities of the wind direction and speed in the considered ocean area. The PDF selection for these variables is challenging owing to the high degree of dispersion of the data. Therefore, a histogram was generated using the PDFs to evaluate the compatibility between the parameters. Figure 6 shows the PDFs considered for the wind parameters (Wind direction and speed).

Next, a GOF test was performed to measure the compatibility of a random sample with several theoretical PDFs. Upon the data distribution, the Kolmogorov–Smirnov (K–S) test (Anderson and Darling 1952) was used to determine the PDF best representing the original data, where the K–S test is based on the maximum absolute difference between the distribution functions of the samples (Lopes et al. 2007). For a given sample (n), the K–S test statistic (D_n) can be calculated using Equation (1).

$$D_n = \sup_x \left| F_n(x) - F(x) \right| \tag{1}$$

where $\sup_x$ is the supremum of the set of distances.

Table 3. K-S method based GOF test results for wind direction and speed

Wind direction (X_1)		Wind speed (X_2)	
Distribution	Goodness-of-Fit	Distribution	Goodness-of-Fit
Exponential	0.2749	Exponential	0.1696
Log-logistic	0.2634	Log-logistic	0.3942
Log-normal	0.2024	Log-normal	0.1314
Normal	**0.0783**	Normal	0.1113
Uniform	0.0977	Uniform	N/A
Weibull	0.0825	**3-parameter Weibull**	**0.0643**

The calculated statistic for each variable is presented in Table 3, where the distribution function with the lowest value of the GOF is selected for the final PDF, i.e., the normal function for wind direction and the 3-parameter Weibull function for wind speed. Equations (2) and (3) represent the PDFs of the wind direction and speed, respectively.

$$f(X_1) = \frac{1}{\sigma\sqrt{2\pi}} \exp\left(-\frac{(X_1 - \mu)^2}{2\sigma^2} \right), \quad \mu = 183.97, \quad \sigma = 88.91 \tag{2}$$

$$f(X_2) = \frac{\alpha}{\beta}\left(\frac{X_2 - \gamma}{\beta} \right)^{\alpha - 1} \exp\left[-\left(\frac{X_2 - \gamma}{\beta} \right)^{\alpha} \right], \quad \alpha = 1.8353, \quad \beta = 6.5835, \quad \gamma = 0.0418 \tag{3}$$

where $f(x)$ = probability density distribution function, μ = mean value, σ = standard deviation, α = scale parameter, β = shape parameter, and γ = location parameter.

3.2 Humidity (X_3)

Level of humidity is characterised from the metocean data at operable ocean sites of the aircraft carrier. In this study, humidity data collected for ten years around the Korean peninsula was used. Table 4 presents the histogram with a bin width of 10% humidity. Table 5 presents the probability density of humidity and Figure 7 shows the histogram and examples of PDFs of humidity. It is found from Table 6 that the 2-parameter Weibull function represents the best fit of the humidity distribution.

$$f\left(X_3\right)=\frac{\alpha}{\beta}\left(\frac{X_3}{\beta}\right)^{\alpha-1}\exp\left[-\left(\frac{X_3}{\beta}\right)^{\alpha}\right],\ \alpha=5.9078,\ \beta=80.4490 \qquad (4)$$

Table 4. Metocean data of humidity for the considered ocean area

Sea	Average humidity (%)										Total
	0–10	10–20	20–30	30–40	40–50	50–60	60–70	70–80	80–90	90–100	
East	0.06	0.02	0.10	2.24	10.49	16.86	15.57	17.28	21.55	15.81	100
South	0.01	0.00	0.01	0.18	1.89	11.11	22.46	19.88	21.58	22.88	100
West	0.00	0.00	0.00	0.20	2.92	12.78	17.08	17.54	25.53	23.96	100
Average	0.02	0.01	0.04	0.87	5.10	13.58	18.37	18.23	22.89	20.88	100

Table 5. Probability density of humidity for the considered ocean area

Wind direction (%)	Probability density
0–10	2.4362E-05
10–20	6.7311E-06
20–30	3.7771E-05
30–40	0.0009
40–50	0.0052
50–60	0.0139
60–70	0.0191
70–80	0.0187
80–90	0.0243
90–100	0.0179

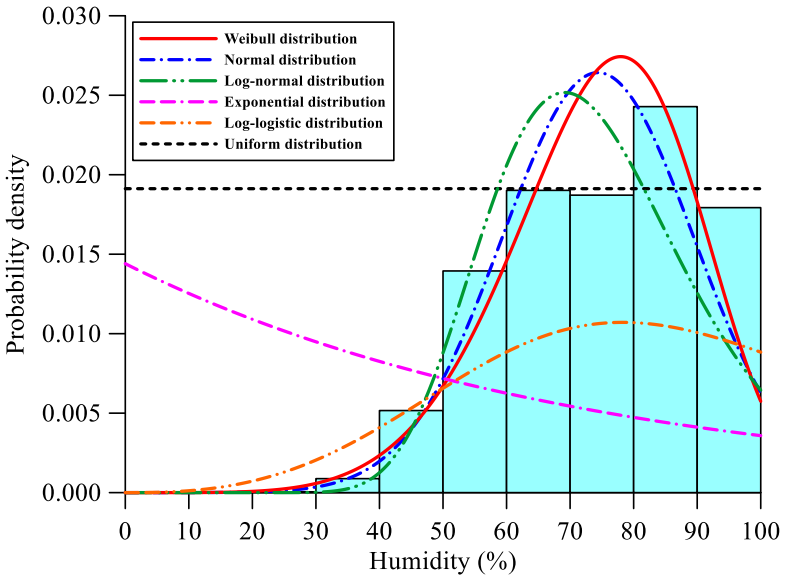

Figure 7. PDF of humidity (*X3*).

Table 6. K-S method based GOF test results for humidity

Humidity (X_3)	
Distribution	Goodness-of-Fit
Exponential	0.4401
Log-logistic	0.4423
Log-normal	0.1364
Normal	0.1265
Uniform	N/A
2-parameter Weibull	**0.1182**

3.3 Leak location (X_4)

The leak location depends on the shape and size of the flight deck of the aircraft carrier. In this study, the flight deck was divided into a number of 62 compartments, as shown in Figure 8. As fuel of aircrafts is the main source of leaks on the flight deck, the locations and movement routes of fixed and rotary-wing aircrafts were investigated. Moreover, a discrete sortie scheme was considered in which eight fixed-wing aircraft and two rotary-wing aircraft were deployed. The PDF for leak location is governed by the process time of the aircraft (Bingol 2016). The discrete time modelling for the activities in the sortie generation process (Faas 2003) and related statistical distributions (Rossetti and McGee 2006; Spencer et al. 2010; Sheppard 2014) are presented in Table 7. For each aircraft, the PDF was calculated based on the sum of the residence time for each compartment by calculating the residence time before take-off, residence time after landing, and transit time between the flight deck and the hangar.

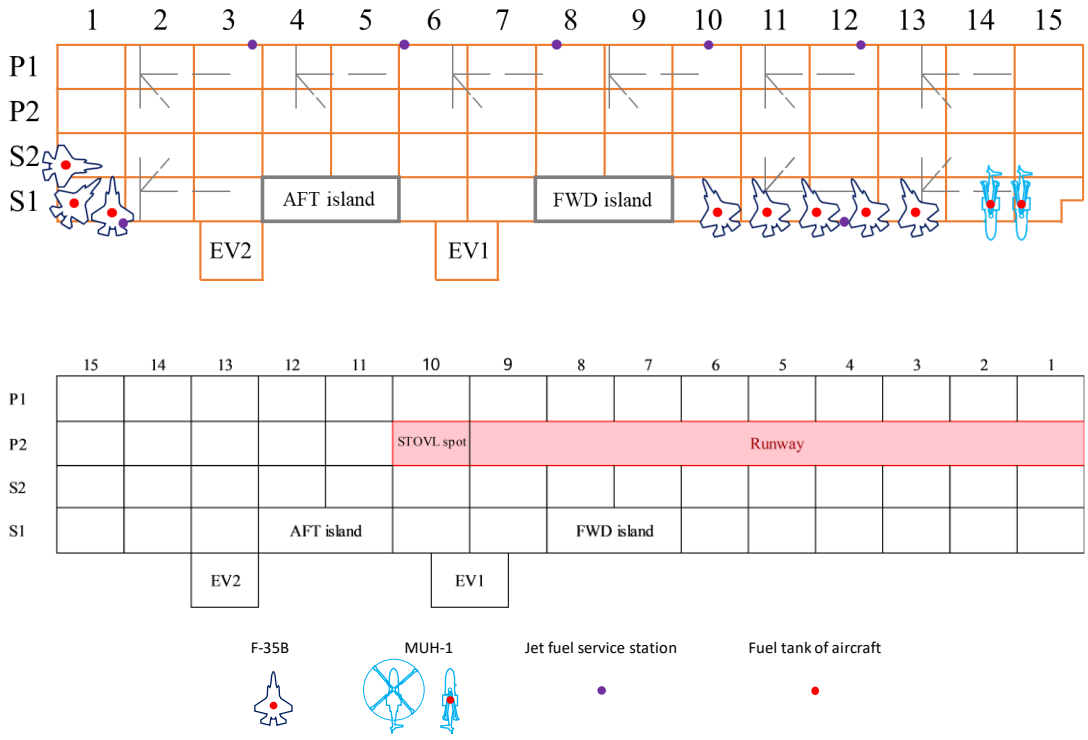

Figure 8. Arrangement of aircrafts on the flight deck.

Table 7. Distributions of the process time and related parameters

Process	Time and distribution	Reference
Refuelling	Normal (0.5, 0.145) h	Spencer et al. (2010)
Other servicing (oil, liquid oxygen, hydraulics, or tyres)	Normal (0.3, 0.087) h	Spencer et al. (2010)
Configuration (weapon loading or pod installation)	Uniform (28, 249) min	Spencer et al. (2010)
Pre-flight inspection	Triangular (50, 60, 70) min	Faas (2003)
Engine start, final systems check, and taxiing	Normal (0.8, 0.232) h	Spencer et al. (2010)
Take-off	Triangular (2, 3, 4) min	Faas (2003)
Sortie	Normal (2, 0.5) h	Faas (2003)
Landing	Triangular (14, 15, 16) min	Faas (2003)
Parking and recovery	Triangular (5, 7, 9) min	Faas (2003)
Basic post-flight operations and aircrew debrief	Normal (2, 0.58) h	Spencer et al. (2010)
Troubleshooting	Triangular (20, 24, 30) min	Faas (2003)
Wait for part(s) to be issued from the supply	Triangular (0.5, 2, 2.5) h	Rossetti & McGee (2006)
Scheduled maintenance	Triangular (5, 7, 8) d	Rossetti & McGee (2006)
Depot level maintenance	Triangular (110, 131, 144) d	Sheppard (2014)

Figure 9 shows the calculations of the residence time for the movement of an aircraft from the hangar to take-off and its movement from landing to the hangar, as an example. The residence time values for all aircrafts were calculated similarly, and the residence time for each compartment is shown in Figure 10.

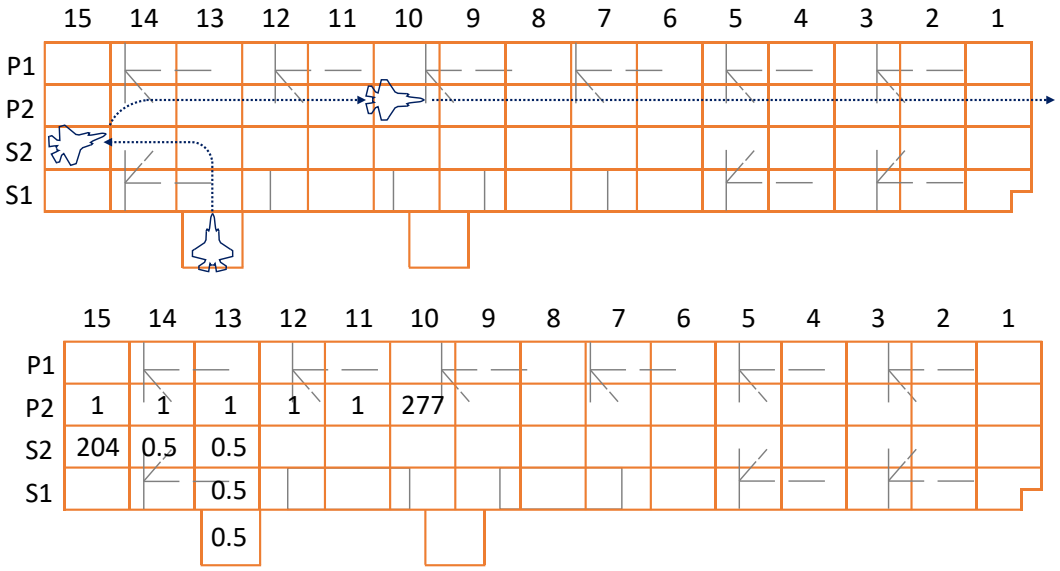

(a) Movement from the hangar to take-off

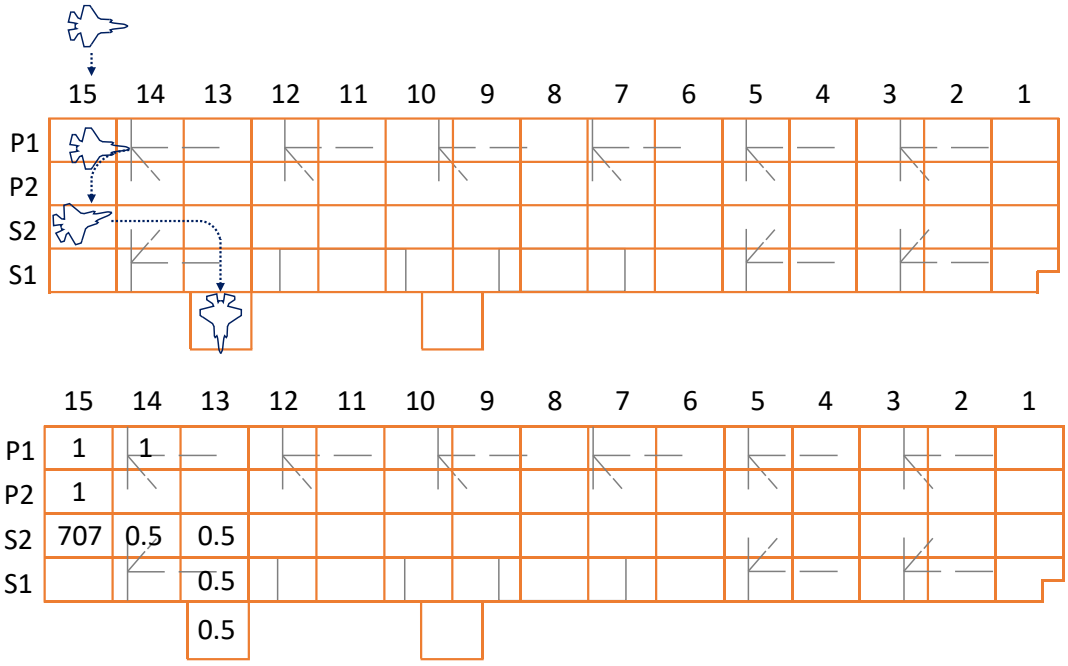

(b) Movement from landing to the hangar

Figure 9. Aircraft movement route and residence time (min).

	Stern 15	14	13	12	11	10	9	8	7	6	5	4	3	2	Bow 1
P1	3.0	3.0	0.0	0.0	0.0	0.0	0.0	0.0	0.0	0.0	2.0	226.5	231.5	0.0	0.0
P2	4.0	3.0	3.0	3.0	3.0	2216.0	7.0	7.0	7.0	8.0	8.0	6.0	10.0	3.0	0.0
S2	915.0	5.0	3.0	0.0	0.0	5.0	12.0	5.0	5.0	7.0	6.0	7.0	8.0	3.0	0.0
S1	1816.0	2.0	3.0	AFT island		0.0	7.0	FWD island		906.0	905.0	1804.0	1137.5	234.5	0.0
			3.0			7.0									<Unit: min>

Figure 10. Total residence time for each compartment on the flight deck for all aircraft.

Table 8 presents the probability density of leak location (*X4*), and Figure 11 shows the histogram and examples of PDFs of leak location. Owing to high data dispersion, the histogram was generated by rearranging the data. Table 9 summarises the K-S method based GOF test results of leak location, and Equation (5) defines the PDF of leak location which follows the normal distribution.

$$f\left(X_4\right)=\frac{1}{\sigma\sqrt{2\pi}}\exp\left[-\frac{\left(X_4-\mu\right)^2}{2\sigma^2}\right],\quad \mu=31.3450,\quad \sigma=2.4792 \tag{5}$$

Table 8. Probability density for leak location

Section	Compartment	Probability density	Section	Compartment	Probability density
0–1	P1_1	0	31–32	P2_10	0.2098
1–2	P1_6	0	32–33	S1_4	0.1708
2–3	P1_8	0	33–34	S2_15	0.0866
3–4	P1_10	0	34–35	S1_5	0.0857
4–5	P1_12	0	35–36	P1_3	0.0219
5–6	P2_1	0	36–37	S2_9	0.0011
6–7	S2_11	0	37–38	S2_3	0.0008
7–8	S1_1	0	38–39	P2_5	0.0008
8–9	S1_8	0	39–40	S2_6	0.0007
9–10	S1_11	0	40–41	P2_9	0.0007
10–11	P1_5	0.0002	41–42	P2_7	0.0007
11–12	P1_14	0.0003	42–43	P2_4	0.0006
12–13	P2_2	0.0003	43–44	S2_10	0.0005
13–14	P2_12	0.0003	44–45	S2_7	0.0005
14–15	P2_14	0.0003	45–46	E2	0.0003
15–16	S2_13	0.0003	46–47	S1_13	0.0003

16–17	E1	0.0003	47–48	S2_2	0.0003
17–18	P2_15	0.0004	48–49	P2_13	0.0003
18–19	S2_8	0.0005	49–50	P2_11	0.0003
19–20	S2_14	0.0005	50–51	P1_15	0.0003
20–21	S2_5	0.0006	51–52	S1_14	0.0002
21–22	P2_8	0.0007	52–53	S1_12	0
22–23	S2_4	0.0007	53–54	S1_10	0
23–24	S1_9	0.0007	54–55	S1_7	0
24–25	P2_6	0.0008	55–56	S2_12	0
25–26	P2_3	0.0009	56–57	S2_1	0
26–27	P1_4	0.0214	57–58	P1_13	0
27–28	S1_2	0.0222	58–59	P1_11	0
28–29	S1_6	0.0858	59–60	P1_9	0
29–30	S1_3	0.1077	60–61	P1_7	0
30–31	S1_15	0.172	61–62	P1_2	0

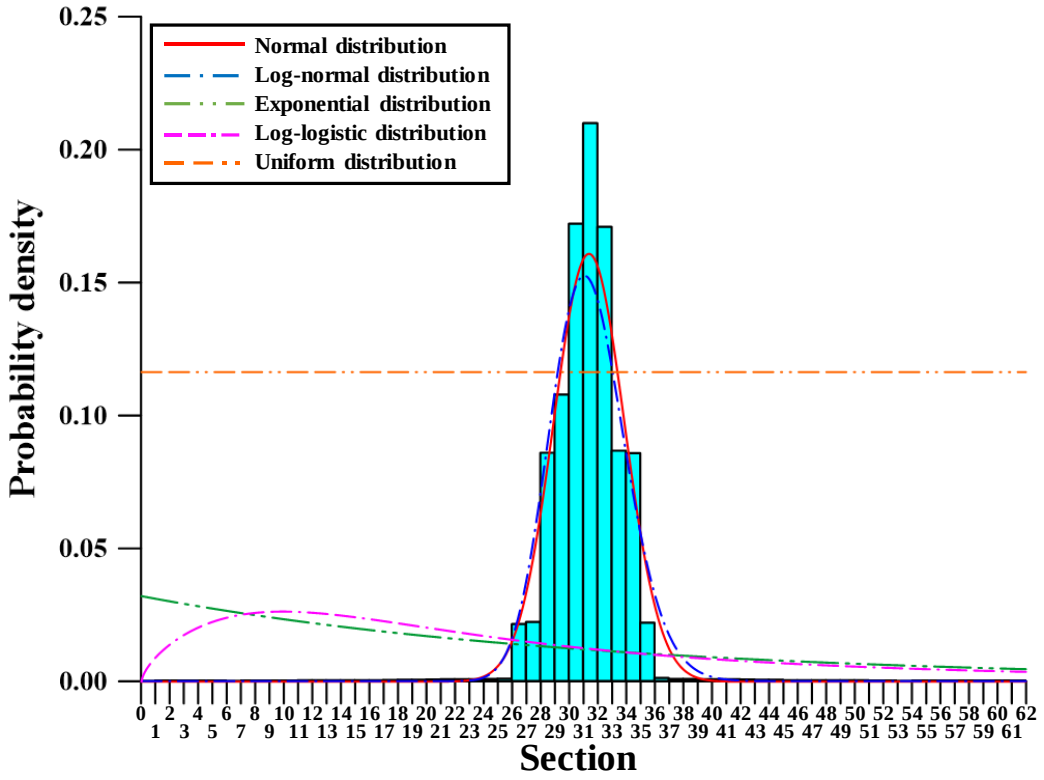

Figure 11. PDF of leak location (X_4).

Table 9. K-S method based GOF test results for leak location

Leak location (X_4)	
Distribution	Goodness-of-Fit
Exponential	0.5628
Log-logistic	0.5465
Log-normal	0.1427
Normal	**0.1217**
Uniform	0.1623
Weibull	N/A

To verify the selected PDF for leak location (X_4), the leak locations considering SGR were compared with the historical data of fire accidents. Table 10 summarises the data for flight deck fire accidents that occurred worldwide during 1944–1981 (Darwin et al. 2005). Figure 12 presents a comparison of the leak locations between historical data and selected PDF where leak locations of fire scenarios indicate the data predicted from the selected PDF. It is confirmed that the selected PDF represents the historical data well.

Table 10. Major fire accidents on aircraft carriers

No.	Date	Ship	Displacement (tonnes)	Cause of fire	No. of fatalities
1	1944.10.	Franklin (CV-13)	27,100	Kamikaze attack	56
2	1944.10.	Belleau wood (CVL-24)	11,000	Kamikaze attack	92
3	1944.11.	Essex (CV-9)	27,100	Kamikaze attack	15
4	1944.12.	Essex (CV-9)	27,100	Aircraft fuel	-
5	1945.01.	Hancock (CV-19)	27,100	Bomb explosion	62
6	1945.04.	Enterprise (CV-6)	21,000	Kamikaze attack	-
7	1945.05.	Bunker Hill (CV-17)	27,100	Kamikaze attack	352
8	1945.05.	Enterprise (CV-6)	21,000	Kamikaze attack	13
9	1945.01.	Ticonderoga (CV-14)	27,100	Kamikaze attack	-
10	1945.03.	Randolph (CV-15)	27,100	Kamikaze attack	25
11	1951.07.	Midway (CV-41)	64,000	Aircraft landing accident	-
12	1951.09.	Essex (CV-9)	27,100	Kamikaze attack	7
13	1953.06	Oriskany (CV-34)	30,800	Bomb explosion	2
14	1953.10.	Leyte (CV-32)	27,100	Hydraulic catapult explosion	37
15	1954.05.	Bennington (CVS-20)	27,100	Hydraulic catapult explosion	106

16	1958.01	Kearsarge (CVS-33)	27,100	Hydraulic catapult explosion	3
17	1958.01	Essex (CV-9)	27,100	Flight deck crash	?
18	1958.01	Hancock (CV-19)	27,100	Bomb explosion	?
19	1959.05	Essex (CV-9)	27,100	Flight deck crash	3
20	1967.07.	Forrestal (CV-59)	59,650	Flight deck conflagration (Zuni rocket across deck)	134
21	1969.01.	Enterprise (CVN-65)	93,970	Flight deck conflagration cart ‘cooked off’ by Zuni	28
22	1981.05.	Nimitz (CVN-68)	97,000	Flight deck crash	14

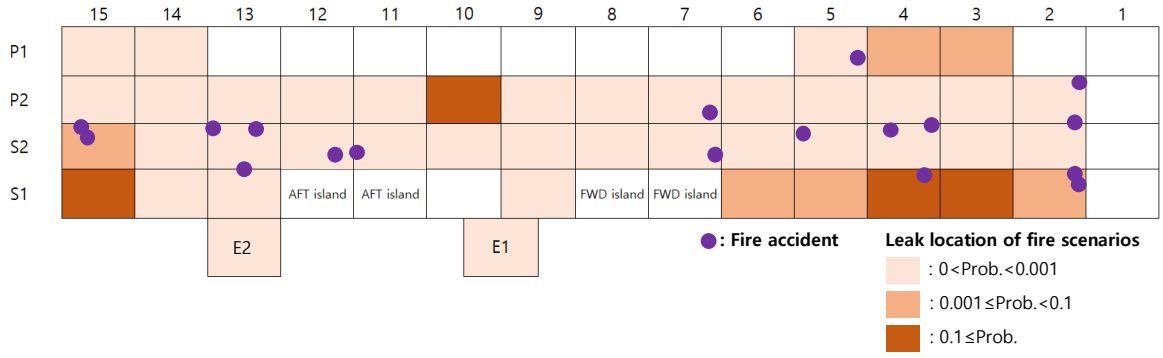

Figure 12. Lak locations in fire scenarios and historical fire accidents.

3.4 Leak amount (X_5)

The leak amount depends on the size of aircraft fuel tanks. Table 11 presents the histogram with a bin width of 10% of leak amount. Equation (6) and Figure 13 show that the PDF for leak amount which follows a uniform distribution. In this study, the GOF test was not performed for leak amount but a uniform distribution function was presumed for the target aircraft carrier as follows:

$$f\left(X_5\right)=C,\quad C=0.01 \tag{6}$$

Table 11. Probability density of leak amount

Leak amount (%)	Probability density
0–10	0.01
10–20	0.01
20–30	0.01
30–40	0.01
40–50	0.01

50–60	0.01
60–70	0.01
70–80	0.01
80–90	0.01
90–100	0.01

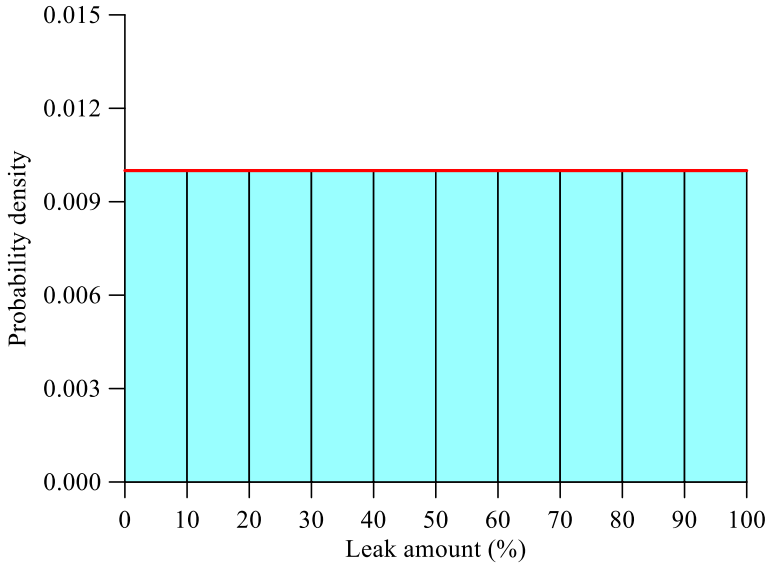

Figure 13. PDF of leak amount (X_5).

3.5 Ship roll and pitch motions (X_6 and X_7)

Ship motions in roll and pitch were considered in association with the operational conditions of the target aircraft carrier. Upon the design criteria of the target ship, the ranges for roll and pitch angles are −15° to 15° and −5° to 5°, respectively. Table 12 presents the histograms with a bin width of 3° and 1° for the roll and pitch angles, respectively. Figure 14 shows the distributions of roll and pitch angles which follow a uniform distribution. In this regard, the variables X_6 and X_7 are represented by a uniform function as follows:

$$f\left(X_6\right)=C\,,\quad C=0.033 \tag{7}$$

$$f\left(X_7\right)=C\,,\quad C=0.1 \tag{8}$$

Table 12(a). Probability density for ship roll angle (X_6)

Rolling angle (°)	Probability density
−15 to −12	0.033
−12 to −9	0.033
−9 to −6	0.033
−6 to −3	0.033
−3 to 0	0.033
0–3	0.033
3–6	0.033
6–9	0.033
9–12	0.033
12–15	0.033

Table 12(b). Probability density for ship pitch angle (X_7)

Pitching angle (°)	Probability density
−5 to −4	0.1
−4 to −3	0.1
−3 to −2	0.1
−2 to −1	0.1
−1 to 0	0.1
0–1	0.1
1–2	0.1
2–3	0.1
3–4	0.1
4–5	0.1

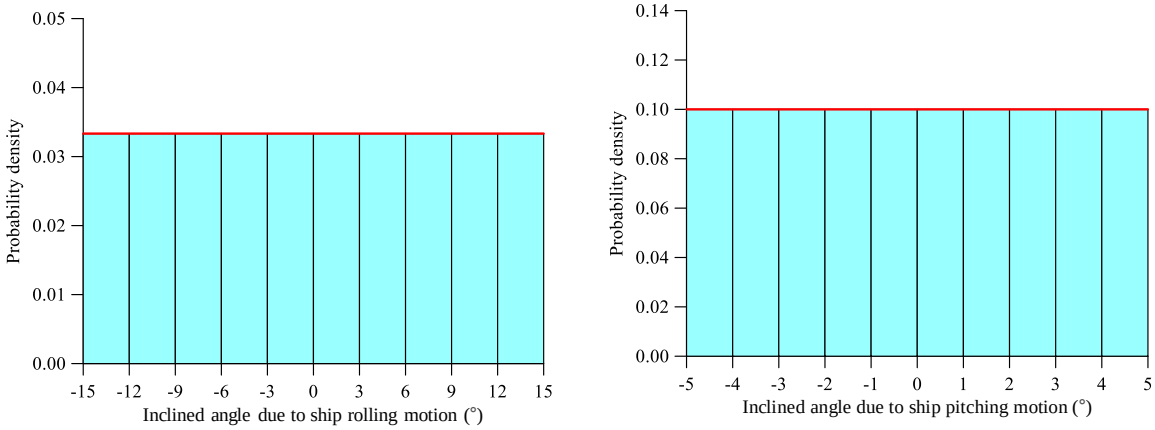

(a) Ship roll motion (X_6) (b) Ship pitch motion (X_7)

Figure 14. Histograms of inclination owing to (a) roll (X_6) and (b) pitch (X_7).

3.6 PDF summary of seven random variables

Probabilistic characteristics of seven random variables have been analysed and their PDFs were defined by the K-S method based GOF test or simple assumptions for the present target ship. As a plenty of historical data together with operational and environmental data become available, more refined characterization of the probability density distributions can be made for random variables. Table 13 summarises the PDFs for all considered parameters of the target ship.

Table 13. PDFs for all considered parameters

Parameter	PDF	Value
Wind direction, X_1	Normal	μ = 183.97, σ = 88.94
Wind speed, X_2	3-parameter Weibull	α = 1.84, β = 6.58, γ = 0.04
Humidity, X_3	2-prameter Weibull	α = 5.91, β = 80.45
Leak location, X_4	Normal	μ = 11.81, σ = 5.07
Leak amount, X_5	Uniform	C = 0.01
Ship roll motion, X_6	Uniform	C = 0.033
Ship pitch motion, X_7	Uniform	C = 0.1

4. Selection of hundred fire scenarios and exceedance diagrams

With the PDFs of seven random variables as obtained in section 3, a total of hundred fire scenarios were selected by a Latin hyper sampling (LHS) technique (Ye 1998; Paik 2020), as indicated in Table 14. Appendix A presents a full listing of the 100 fire scenarios.

Table 14. A total of 100 fire scenarios selected for the flight deck of the target ship

Scenario No.	X_1 Wind direction (°)	X_2 Wind speed (m/s)	X_3 Humidity (%)	X_4 Leak location	X_5 Leak amount (%)	X_6 Roll angle (°)	X_7 Pitch angle (°)	X_8 Leak area (m^2)

1	271.7	0.4	75.3	S1_5	36.5	−3.4	−0.3	24.2
2	8.0	6.5	71.6	S1_3	94.5	10.1	−1.9	9.7
3	252.8	4.0	55.2	P2_6	80.5	0.8	2.9	124.4
4	160.9	5.1	31.4	S1_3	31.5	5.0	−4.3	4.1
5	180.3	6.3	84.0	S2_15	98.5	−12.7	−4.9	69.3
6	59.9	2.5	88.8	S1_2	69.5	−6.1	2.7	45.7
7	229.2	0.9	67.9	S1_2	37.5	−0.7	3.6	17.1
8	173.9	1.4	68.3	P1_3	19.5	4.4	−1.8	15.8
9	156.4	2.1	45.5	S1_15	23.5	−12.4	3.0	55.6
10	258.7	4.1	77.1	S1_3	43.5	−12.1	−1.4	57.4
11	222.0	4.3	65.1	S1_15	74.5	−13.6	−3.7	94.4
12	311.4	5.1	86.5	S1_6	2.5	6.8	−4.8	1.6
13	193.1	10.3	64.0	P2_10	82.5	−11.5	−4.4	36.0
14	137.8	4.5	85.2	P2_10	25.5	13.4	0.0	15.5
15	104.8	3.3	90.9	S2_9	15.5	−4.9	2.6	10.1
16	113.9	8.5	50.7	S1_15	66.5	2.0	3.4	11.2
17	236.6	1.7	92.1	S1_4	67.5	−5.5	−4.5	53.3
18	98.3	6.9	99.3	S1_4	78.5	13.7	−2.3	15.2
19	165.2	13.6	61.2	S1_5	16.5	−9.1	−0.7	19.5
20	317.7	1.8	78.2	S1_15	75.5	14.0	−1.2	15.4
⋮	⋮	⋮	⋮	⋮	⋮	⋮	⋮	⋮
100	332.8	4.7	81.8	P2_10	8.5	−14.8	−0.2	39.9

Note: P = port side, S = starboard side.

In Table 14, a new parameter X_8 is introduced, representing the fire-impacted (leak) area which is useful to determine a safety criterion equivalent to the design fire accidental load (DFAL) for the safety design and engineering of structural systems. Notably, values for the fire-impacted (leak) area (X_8) were determined considering leak location (X_4), leak amount (X_5) and ship roll and pitch motions (X_6 and X_7). The value of X_8 is calculated as follows:

$$X_8 = B(\theta, V) L_{leak} \tag{9}$$

where B = leak breadth (m) which is a function of θ and V, θ = inclined angle calculated from roll and pitch angles (°), V = leak amount or volume (m^3) and L_{leak} = leak length (m).

In this study, the target ship carries F-35B (Lockheed Marin: www.lockheedmartin.com) type aircrafts which are supposed for short take-off/vertical landing. The fuel tank capacity of the aircraft was assumed to be 7,562 L, and the leak amount (volume) was obtained by multiplying the fuel tank capacity with ratio of the leak amount (X_5) in each scenario. The leak length was calculated as the distance from the leak location(X_4) to the edge of the flight deck parallel to the spill direction (combination of X_6 and X_7).

The fire exceedance diagrams are established by the relation between the fire-impacted (leak) area, X_8 versus the exceedance of fire frequency for the 100 fire scenarios as the fire frequency is defined as follows:

$$F_F = F_L P_I \tag{10}$$

where F_F is the fire frequency, $F_L = F_A P_{LL}$ is the leak frequency, F_A is the frequency of the aircraft accident, P_{LL} is the probability of leak location, and P_I is the probability of ignition.

A total of eleven F-35B accidents on the flight deck have been reported for 21 years and thus the aircraft accident frequency F_A is taken as 0.5238 per year (Air Force Safety Center 2022). The probability of leak location probabilities is defined in Table 8.

The ignition probability for a flight deck depends on the ignition type and source. In this study, the ignition probability for each scenario was calculated using the ignition models of Ronza et al. (2007) and Cox (1990). Ronza et al. (2007) analysed a large number of records in hydrocarbon spills and developed a relationship between ignition probability and flash temperature of the spilled hydrocarbon as shown in Table 15. Cox et al. (1990) suggested the ignition probability of gases and liquids as a step-function of the leak flow rate, as indicated in Table 15. Although these ignition models do not consider facility-specific factors (e.g., layout, shape) and ignition speed (e.g., immediate or delayed ignition), they are well adopted for industry applications.

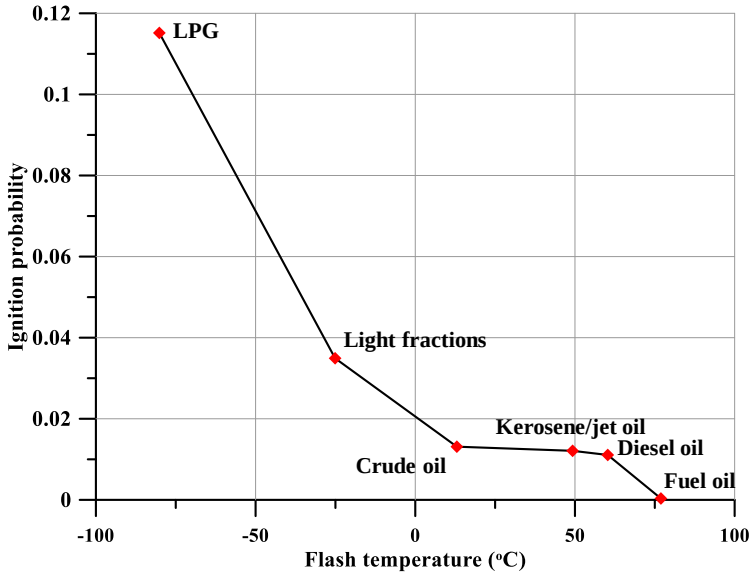

Figure 15. The Ronza ignition model.

Table 15. The Cox ignition model

Leak size	Ignition probability		Probability of explosion given ignition
	Gas	Liquid	
Minor (≤ 1 kg/s)	0.01	0.01	0.04
Major (1–50 kg/s)	0.07	0.03	0.12
Massive (≥ 50 kg/s)	0.3	0.08	0.3

With leak frequency and ignition probability known, the fire frequency can be defined. Table 16 presents the fire frequency calculations for the selected fire scenarios. The calculated fire frequencies for 100 fire scenarios are listed in Appendix B. Figure 16 shows the distribution of the fire frequencies on the flight deck. It is found from Figure 16 that the maximum fire frequency occurs at the compartment P2-10 between AFT and FWD islands which is a short take-off or vertical landing area of aircrafts and it is estimated as 0.020753 by the Ronza ignition model and 0.048364 by the Cox ignition model. While Paik (2020) is referred to for the details of the process to establish exceedance diagrams, Figure 17 shows the fire exceedance diagrams of the leak (fire-impacted) area. If a risk acceptance criterion with an acceptable frequency of 10^{-3} is adopted, the critical leak area is determined from Figure 17 as 115 m^2.

Table 16. Calculation of the fire frequencies for 100 fire scenarios

Scenario No.	Leak area (m^2)	Leak frequency (per year)	Ignition probability by the Ronza model	Ignition probability by the Cox model	Fire frequency by the Ronza model	Fire frequency by the Cox model
1	24.2	0.0449	0.0118	0.03	5.297×10^{-4}	1.347×10^{-3}
2	9.7	0.0564	0.0118	0.03	6.658×10^{-4}	1.693×10^{-3}
3	124.4	0.0008	0.0118	0.03	8.939×10^{-6}	2.273×10^{-5}
4	4.1	0.0564	0.0118	0.03	6.658×10^{-4}	1.693×10^{-3}
5	69.3	0.0454	0.0118	0.03	5.356×10^{-4}	1.362×10^{-3}
6	45.7	0.0116	0.0118	0.03	1.373×10^{-4}	3.490×10^{-4}
7	17.1	0.0116	0.0118	0.03	1.373×10^{-4}	3.490×10^{-4}
8	15.8	0.0115	0.0118	0.03	1.355×10^{-4}	3.445×10^{-4}
9	55.6	0.0901	0.0118	0.03	1.063×10^{-3}	2.702×10^{-3}
10	57.4	0.0564	0.0118	0.03	6.658×10^{-4}	1.693×10^{-3}
11	94.4	0.0901	0.0118	0.03	1.063×10^{-3}	2.702×10^{-3}
12	1.6	0.0858	0.0118	0.01	1.012×10^{-3}	8.580×10^{-4}
13	36.0	0.1099	0.0118	0.03	1.297×10^{-3}	3.298×10^{-3}
14	15.5	0.1099	0.0118	0.03	1.297×10^{-3}	3.298×10^{-3}
15	10.1	0.0006	0.0118	0.03	7.024×10^{-6}	1.786×10^{-5}
16	11.2	0.0901	0.0118	0.03	1.063×10^{-3}	2.702×10^{-3}
17	53.3	0.0895	0.0118	0.03	1.056×10^{-3}	2.684×10^{-3}
18	15.2	0.0895	0.0118	0.03	1.056×10^{-3}	2.684×10^{-3}
19	19.5	0.0449	0.0118	0.03	5.297×10^{-4}	1.347×10^{-3}
20	15.4	0.0901	0.0118	0.03	1.063×10^{-3}	2.702×10^{-3}
⋮	⋮	⋮	⋮	⋮	⋮	⋮
100	39.9	0.1099	0.0118	0.03	1.297×10^{-3}	3.298×10^{-3}

Stern

	15	14	13	12	11	10	9	8	7	6	5	4	3	2	1
P1	0	0	0	0	0	0	0	0	0	0	0	0.000265	0.000542	0	0
P2	0	0	0	0	0	0.020753	0	0	0	0.000009	0	0	0.000006	0	0
S2	0.005891	0	0	0	0	0	0.000021	0	0	0	0	0	0	0	0
S1	0.015944	0	0	AFT island		0	0	FWD island		0.008099	0.004238	0.014783	0.007989	0.000686	0
			0			0									

Bow

(a) Fire frequencies obtained using the Ronza ignition model

	Stern														Bow
	15	14	13	12	11	10	9	8	7	6	5	4	3	2	1
P1	0	0	0	0	0	0	0	0	0	0	0	0.000674	0.001378	0	0
P2	0	0	0	0	0	0.048364	0	0	0	0.000023	0	0	0.000015	0	0
S2	0.014977	0	0	0	0	0	0.000054	0	0	0	0	0	0	0	0
S1	0.040535	0	0	AFT island		0	0	FWD island		0.018875	0.010774	0.035793	0.020312	0.001512	0
			0			0									

(b) Fire frequencies obtained using the Cox ignition model

Figure 16. Fire frequencies (per year) for each compartment on the flight deck.

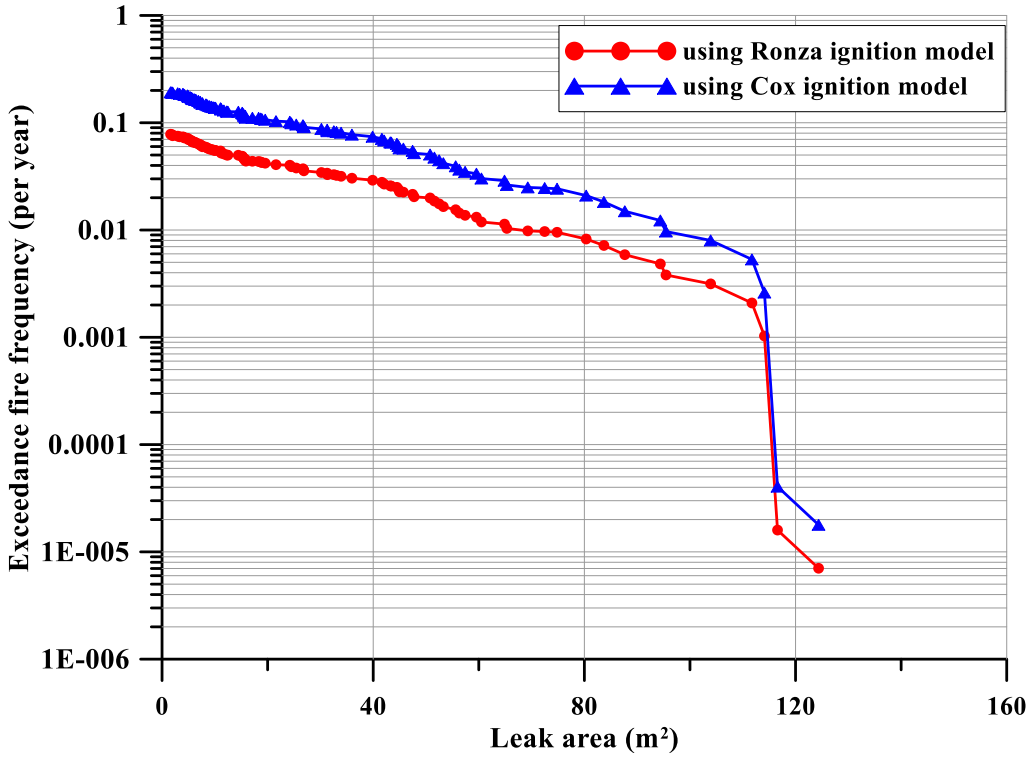

Figure 17. Exceedance fire diagram of the fire-impacted (leak) area.

6. Concluding remarks

A number of seven random parameters, namely wind direction, wind speed, humidity, oil/gas leak location, oil/gas leak amount, ship roll angle and ship pitch angle were considered to represent fire hazards on the flight deck of aircraft carriers. The probability density distribution for each of the seven random parameters was characterized based on operational and ocean environmental database and the corresponding best-fitted function was formulated. Probabilistic sampling technique was used to select a set of hundred fire scenarios on the flight deck of a short-take-off/vertical-landing (STOVL) type Queen Elizabeth (QE) class aircraft

carrier. Exceedance diagrams of the fire frequency were established against the fire-impacted area when the target ship carries F-35B aircrafts which are purposed for STOVL.

The results obtained from the present fire safety studies can be useful for fire safety design and engineering on the flight deck of STOVL aircraft carriers, where the recoverability of firefighting systems should be improved to ensure a high degree of synergy and interdependency between the vulnerability and recoverability requirements and resulting design features.

Acknowledgements

The authors acknowledge the financial support provided by the Defence Industry Technology Center (DITC) of Korea (Project code 912849501).

ORCID

Jeom Kee Paik http://orcid.org/0000-0003-2956-9359

References

Air Force Safety Center. 2022. F-35 Flight mishap history. (https://www.safety.af.mil/)

Anderson TW, Darling DA. 1952. Asymptotic theory of certain "goodness-of-fit" criteria based on stochastic processes. Annals of Mathematical Statistics. 23:193–212.

BAE Systems. 2022. Queen Elizabeth (QE) Class Aircraft Carrier. (https://www.baesystems.com/en-uk/product/aircraft-carriers)

Bingol G. 2016. Simulation of aircraft sortie generation under an autonomic logistics system. Air Force Institute of Technology. Wright-Patterson Air Force Base, Ohio.

Chung K, Kim M, Han Y, Nguyen LD. 2021. Validation of methods for estimation of the heat flux into the liquid nitrogen pool from the concrete ground. Journal of Advanced Marine Engineering and Technology. 45(1):1-9.

Cox AW, Lees FP, Ang ML. 1990. Classification of hazardous locations. Institution of Chemical Engineers. UK.

Darwin R, Bowman H, Hunstad M, Leach W, Williams F. 2005. Aircraft carrier flight and hangar deck fire protection: history and current status. Naval Air Warfare Center Weapons Division. CA.

DNV. 2015. Offshore standard: helicopter decks. Report No. DNV-OS-E401. Det Norske Veritas, Oslo, Norway.

Fass PD. 2003. Simulation of an autonomic system. MS Thesis: AFIT/GOP/ENS/03-07: Air Force Institute of Technology. Wright-Patterson Air Force Base, Ohio.

IMO. 2015. Construction–Fire protection, fire detection and fire extinction. International Convention for the Safety of Life at Sea: International Maritime Organization: UK.

Kim SJ, Lee J, Paik JK, Seo JK, Shin WH, Park JS. 2016. A study on fire design accidental loads for aluminum safety helidecks. International Journal of Naval Architecture and Ocean Engineering. 8: 519-529.

Lee H. 2021. Application of JP-5 in a CRDI diesel engine with various fuel injection distribution strategy. Journal of Advanced Marine Engineering and Technology. 45(5): 243-251.

Leonard JT, Fulper CR, Darwin R, Back GG, Burns RE, Ouelette R. 1992. Fire hazards of Mixed fuels on the flight deck (NRL/MR-6180-92-6975). Naval Research Laboratory. Washington DC. USA.

Lopes RHC, Reid ID, Hobson PR. 2007. The two-dimensional Kolmogorov-Smirnov test. XI International Workshop on Advanced Computing and Analysis Techniques in Physics Research. Netherlands: Amsterdam.

Nolan DP. 1996. Handbook of fire and explosion protection engineering principles for oil, gas, chemical, and related facilities. Noyes Publications.

Paik JK. 2020. Advanced structural safety studies with extreme conditions and accidents. Singapore: Springer.

Paik JK. 2022. Ship-shaped offshore installations: design, construction, operation, healthcare and decommissioning. Second edition. Cambridge, UK: Cambridge University Press.

Ronza A, Vilchez JA, Casal J. 2007. Using transportation accident databases to investigate ignition and explosion probabilities of flammable spills. Journal of Hazardous Material. 146:106–123.

Rossetti MD, McGee JB. 2006. Modeling sortie generation for unit-level logistics planners. Report, AFRL-HE-WP-TR-2006-0058: Air Force Research Laboratory. OH.

Sheppard WA. 2014. Simulating F-22 heavy maintenance and modifications workforce multi-skilling. MS Thesis: AFIT-ENS-14-M-28: Air Force Institute of Technology. Wright-Patterson Air Force Base, Ohio.

Spencer K, Hall R, Ostrander M. 2010. US Air force maintenance capability and capacity modeling and simulation summary technical report (U). Information Assurance Technology Analysis Center.

Ye KQ. 1998. Orthogonal column Latin hypercubes and their application in computer experiments. Journal of the American Statistical Association. 93(444):1430–1439.

Appendix A. Selection of 100 probabilistic fire scenarios on the flight deck

Scenario No.	X1	X2	X3	X4	X5	X6	X7	X8
	Wind direction (°)	Wind speed (m/s)	Humidity (%)	Leak location	Leak amount (%)	Roll angle (°)	Pitch angle (°)	Leak area (m^2)
1	271.7	0.4	75.3	S1_5	36.5	−3.4	−0.3	24.2
2	8.0	6.5	71.6	S1_3	94.5	10.1	−1.9	9.7
3	252.8	4.0	55.2	P2_6	80.5	0.8	2.9	124.4
4	160.9	5.1	31.4	S1_3	31.5	5.0	−4.3	4.1
5	180.3	6.3	84.0	S2_15	98.5	−12.7	−4.9	69.3
6	59.9	2.5	88.8	S1_2	69.5	−6.1	2.7	45.7
7	229.2	0.9	67.9	S1_2	37.5	−0.7	3.6	17.1
8	173.9	1.4	68.3	P1_3	19.5	4.4	−1.8	15.8
9	156.4	2.1	45.5	S1_15	23.5	−12.4	3.0	55.6
10	258.7	4.1	77.1	S1_3	43.5	−12.1	−1.4	57.4
11	222.0	4.3	65.1	S1_15	74.5	−13.6	−3.7	94.4
12	311.4	5.1	86.5	S1_6	2.5	6.8	−4.8	1.6
13	193.1	10.3	64.0	P2_10	82.5	−11.5	−4.4	36.0
14	137.8	4.5	85.2	P2_10	25.5	13.4	0.0	15.5
15	104.8	3.3	90.9	S2_9	15.5	−4.9	2.6	10.1
16	113.9	8.5	50.7	S1_15	66.5	2.0	3.4	11.2
17	236.6	1.7	92.1	S1_4	67.5	−5.5	−4.5	53.3
18	98.3	6.9	99.3	S1_4	78.5	13.7	−2.3	15.2
19	165.2	13.6	61.2	S1_5	16.5	−9.1	−0.7	19.5
20	317.7	1.8	78.2	S1_15	75.5	14.0	−1.2	15.4
21	206.2	7.4	49.2	P2_10	10.5	11.6	−4.0	30.2
22	119.6	3.8	60.6	S1_4	87.5	−1.0	4.0	83.7
23	342.2	5.9	67.0	S1_5	30.5	−9.7	2.1	31.3
24	286.8	3.8	92.7	S1_4	46.5	−6.7	2.0	31.3
25	107.9	3.5	81.0	S2_15	17.5	8.9	0.9	8.3
26	239.2	9.3	77.5	S1_2	1.5	11.3	−2.2	3.9
27	201.8	3.7	80.3	S1_15	65.5	6.2	−1.3	5.8
28	217.4	2.0	69.6	S1_4	89.5	−13.9	0.5	111.7
29	226.7	2.2	95.0	S1_15	90.5	7.1	0.3	7.6
30	199.6	11.1	70.8	S1_15	53.5	−8.5	4.8	47.7
31	79.4	8.2	74.9	S1_15	11.5	11.0	−4.6	5.6
32	47.4	5.7	86.9	S1_15	58.5	−3.7	−3.5	11.7
33	147.3	5.2	70.0	S2_9	76.5	−0.1	0.8	186.9
34	111.0	5.8	93.4	S1_15	57.5	2.6	−2.7	7.2
35	215.1	1.1	87.4	P2_10	5.5	13.1	−3.9	45.0
36	184.6	3.3	91.5	S2_15	81.5	−4.6	0.2	33.9
37	241.8	4.8	88.3	S1_4	3.5	8.3	3.3	1.8
38	208.4	9.0	59.2	P2_10	4.5	−10.9	−2.4	11.2
39	191.0	7.5	57.7	S1_6	68.5	0.5	3.8	44.8
40	75.0	3.6	77.8	S1_15	20.5	14.3	−0.9	12.2
41	40.0	4.2	73.1	S1_4	47.5	3.8	0.4	4.3
42	182.5	1.9	84.4	S1_5	27.5	−9.4	−0.8	26.7
43	87.5	10.1	75.7	P1_4	99.5	10.7	0.7	72.5
44	353.5	12.9	82.5	P2_10	79.5	−13.0	−3.2	41.6
45	247.2	7.3	64.6	S1_3	62.5	−8.8	−2.0	44.5
46	167.4	3.0	39.3	P1_3	13.5	1.4	3.5	14.4
47	291.1	7.1	53.1	S1_15	97.5	8.0	1.4	8.6
48	83.5	17.1	94.2	S1_4	50.5	−10.3	2.8	47.5

49	130.3	2.8	87.8	S1_6	61.5	−2.8	−4.1	65.3
50	169.6	5.3	52.0	S1_15	93.5	−13.3	3.7	114.1
51	295.6	2.9	42.9	S2_15	21.5	11.9	1.6	18.7
52	54.0	5.5	98.0	S2_15	73.5	9.8	4.2	26.9
53	197.5	6.7	67.4	S1_3	32.5	−14.2	−3.8	103.9
54	163.1	9.5	72.7	S1_4	48.5	5.6	−3.1	5.0
55	255.7	5.6	62.4	S1_5	70.5	7.7	−1.5	6.4
56	186.7	2.6	78.5	S1_4	29.5	−2.5	1.8	25.4
57	65.3	7.0	79.2	P2_10	49.5	1.7	4.4	60.5
58	268.3	2.4	84.8	P2_10	44.5	14.6	2.4	80.3
59	116.8	5.4	56.1	S1_3	35.5	1.1	−1.6	6.3
60	101.6	0.7	47.5	S2_15	63.5	−0.4	−1.0	10.0
61	275.2	2.7	66.0	S1_3	9.5	9.5	3.1	3.0
62	219.7	3.4	68.7	S1_2	52.5	−8.2	−4.2	43.4
63	158.6	7.7	82.9	P2_10	18.5	−7.3	1.2	6.9
64	261.8	1.3	58.5	P2_10	45.5	12.8	−2.6	51.6
65	91.2	8.7	85.6	P1_4	7.5	−14.5	1.9	12.5
66	300.5	8.1	95.9	P2_3	85.5	−4.0	4.6	32.5
67	140.2	6.4	72.0	S2_15	59.5	12.2	3.9	33.1
68	151.9	9.9	83.6	S2_9	12.5	4.1	−3.4	6.1
69	127.7	5.0	59.9	S1_6	64.5	−5.8	−2.8	43.2
70	212.8	11.5	81.4	S1_4	71.5	8.6	−2.9	7.3
71	171.7	9.1	74.6	S1_6	60.5	−1.3	4.3	95.5
72	94.8	9.7	65.6	S2_15	51.5	6.5	−3.3	15.9
73	154.2	7.2	74.2	S1_6	33.5	10.4	−0.1	5.0
74	188.9	11.9	73.9	S1_4	34.5	5.3	1.5	3.4
75	31.4	4.4	76.0	S1_2	22.5	−1.6	0.1	18.3
76	122.4	2.3	83.3	S1_5	84.5	−10.0	−3.0	64.9
77	244.4	5.7	66.5	S2_15	39.5	−7.0	0.6	18.9
78	144.9	8.4	86.1	S1_3	83.5	4.7	2.2	7.6
79	70.3	4.9	61.8	S1_4	41.5	−6.4	−0.4	26.8
80	132.8	10.6	63.0	S2_15	6.5	−4.3	−1.7	4.8
81	204.0	8.0	69.2	S1_6	77.5	−1.9	4.5	116.6
82	265.0	6.0	79.6	S1_3	91.5	3.2	2.3	9.3
83	234.1	8.8	70.4	P2_10	28.5	14.9	−3.6	87.7
84	249.9	6.1	80.7	P1_3	95.5	5.9	5.0	74.8
85	278.9	4.6	76.4	S1_5	38.5	0.2	4.7	50.8
86	178.2	1.6	73.5	S1_5	26.5	−11.8	4.9	59.5
87	195.3	4.2	71.2	P2_10	40.5	9.2	−2.1	24.5
88	305.7	4.7	54.2	P2_10	42.5	−10.6	4.1	21.6
89	282.7	6.6	80.0	S1_3	55.5	2.9	1.7	5.7
90	324.7	6.8	82.1	S1_3	54.5	7.4	−2.5	5.4
91	210.6	7.9	56.9	S1_3	72.5	12.5	1.0	11.1
92	21.1	3.2	90.3	S2_15	92.5	3.5	−4.7	15.2
93	231.6	7.6	89.8	S1_6	24.5	−11.2	3.2	42.1
94	125.0	14.6	96.9	S1_4	88.5	−3.1	−0.5	52.5
95	135.3	3.1	78.9	P1_3	14.5	−2.2	−0.6	2.0
96	149.6	10.8	72.4	S1_15	96.5	2.3	−1.1	8.9
97	176.0	3.9	89.3	P2_10	0.5	−5.2	1.3	2.0
98	224.4	6.2	76.7	S1_15	86.5	−7.9	2.5	56.3
99	142.6	12.3	63.5	P2_10	56.5	−7.6	1.1	15.8
100	332.8	4.7	81.8	P2_10	8.5	−14.8	−0.2	39.9

Appendix B. Calculation of the fire frequencies for 100 fire scenarios

Scenario No.	Leak area (m^2)	Leak frequency (per year)	Ignition probability by the Ronza model	Ignition probability by the Cox model	Fire frequency by the Ronza model	Fire frequency by the Cox model
1	24.2	0.0449	0.0118	0.03	5.297×10^{-4}	1.347×10^{-3}
2	9.7	0.0564	0.0118	0.03	6.658×10^{-4}	1.693×10^{-3}
3	124.4	0.0008	0.0118	0.03	8.939×10^{-6}	2.273×10^{-5}
4	4.1	0.0564	0.0118	0.03	6.658×10^{-4}	1.693×10^{-3}
5	69.3	0.0454	0.0118	0.03	5.356×10^{-4}	1.362×10^{-3}
6	45.7	0.0116	0.0118	0.03	1.373×10^{-4}	3.490×10^{-4}
7	17.1	0.0116	0.0118	0.03	1.373×10^{-4}	3.490×10^{-4}
8	15.8	0.0115	0.0118	0.03	1.355×10^{-4}	3.445×10^{-4}
9	55.6	0.0901	0.0118	0.03	1.063×10^{-3}	2.702×10^{-3}
10	57.4	0.0564	0.0118	0.03	6.658×10^{-4}	1.693×10^{-3}
11	94.4	0.0901	0.0118	0.03	1.063×10^{-3}	2.702×10^{-3}
12	1.6	0.0858	0.0118	0.01	1.012×10^{-3}	8.580×10^{-4}
13	36.0	0.1099	0.0118	0.03	1.297×10^{-3}	3.298×10^{-3}
14	15.5	0.1099	0.0118	0.03	1.297×10^{-3}	3.298×10^{-3}
15	10.1	0.0006	0.0118	0.03	7.024×10^{-6}	1.786×10^{-5}
16	11.2	0.0901	0.0118	0.03	1.063×10^{-3}	2.702×10^{-3}
17	53.3	0.0895	0.0118	0.03	1.056×10^{-3}	2.684×10^{-3}
18	15.2	0.0895	0.0118	0.03	1.056×10^{-3}	2.684×10^{-3}
19	19.5	0.0449	0.0118	0.03	5.297×10^{-4}	1.347×10^{-3}
20	15.4	0.0901	0.0118	0.03	1.063×10^{-3}	2.702×10^{-3}
21	30.2	0.1099	0.0118	0.03	1.297×10^{-3}	3.298×10^{-3}
22	83.7	0.0895	0.0118	0.03	1.056×10^{-3}	2.684×10^{-3}
23	31.3	0.0449	0.0118	0.03	5.297×10^{-4}	1.347×10^{-3}
24	31.3	0.0895	0.0118	0.03	1.056×10^{-3}	2.684×10^{-3}
25	8.3	0.0454	0.0118	0.03	5.356×10^{-4}	1.362×10^{-3}
26	3.9	0.0116	0.0118	0.01	1.373×10^{-4}	1.163×10^{-4}
27	5.8	0.0901	0.0118	0.03	1.063×10^{-3}	2.702×10^{-3}
28	111.7	0.0895	0.0118	0.03	1.056×10^{-3}	2.684×10^{-3}
29	7.6	0.0901	0.0118	0.03	1.063×10^{-3}	2.702×10^{-3}
30	47.7	0.0901	0.0118	0.03	1.063×10^{-3}	2.702×10^{-3}
31	5.6	0.0901	0.0118	0.03	1.063×10^{-3}	2.702×10^{-3}
32	11.7	0.0901	0.0118	0.03	1.063×10^{-3}	2.702×10^{-3}
33	186.9	0.0006	0.0118	0.03	7.024×10^{-6}	1.786×10^{-5}
34	7.2	0.0901	0.0118	0.03	1.063×10^{-3}	2.702×10^{-3}
35	45.0	0.1099	0.0118	0.03	1.297×10^{-3}	3.298×10^{-3}
36	33.9	0.0454	0.0118	0.03	5.356×10^{-4}	1.362×10^{-3}
37	1.8	0.0895	0.0118	0.01	1.056×10^{-3}	8.948×10^{-4}

38	11.2	0.1099	0.0118	0.01	1.297×10^{-3}	1.099×10^{-3}
39	44.8	0.0858	0.0118	0.03	1.012×10^{-3}	2.574×10^{-3}
40	12.2	0.0901	0.0118	0.03	1.063×10^{-3}	2.702×10^{-3}
41	4.3	0.0895	0.0118	0.03	1.056×10^{-3}	2.684×10^{-3}
42	26.7	0.0449	0.0118	0.03	5.297×10^{-3}	1.347×10^{-3}
43	72.5	0.0112	0.0118	0.03	1.326×10^{-3}	3.370×10^{-3}
44	41.6	0.1099	0.0118	0.03	1.297×10^{-3}	3.298×10^{-3}
45	44.5	0.0564	0.0118	0.03	6.658×10^{-4}	1.693×10^{-3}
46	14.4	0.0115	0.0118	0.03	1.355×10^{-4}	3.445×10^{-4}
47	8.6	0.0901	0.0118	0.03	1.063×10^{-3}	2.702×10^{-3}
48	47.5	0.0895	0.0118	0.03	1.056×10^{-3}	2.684×10^{-3}
49	65.3	0.0858	0.0118	0.03	1.012×10^{-3}	2.574×10^{-3}
50	114.1	0.0901	0.0118	0.03	1.063×10^{-3}	2.702×10^{-3}
51	18.7	0.0454	0.0118	0.03	5.356×10^{-4}	1.362×10^{-3}
52	26.9	0.0454	0.0118	0.03	5.356×10^{-4}	1.362×10^{-3}
53	103.9	0.0564	0.0118	0.03	6.658×10^{-4}	1.693×10^{-3}
54	5.0	0.0895	0.0118	0.03	1.056×10^{-3}	2.684×10^{-3}
55	6.4	0.0449	0.0118	0.03	5.297×10^{-4}	1.347×10^{-3}
56	25.4	0.0895	0.0118	0.03	1.056×10^{-3}	2.684×10^{-3}
57	60.5	0.1099	0.0118	0.03	1.297×10^{-3}	3.298×10^{-3}
58	80.3	0.1099	0.0118	0.03	1.297×10^{-3}	3.298×10^{-3}
59	6.3	0.0564	0.0118	0.03	6.658×10^{-4}	1.693×10^{-3}
60	10.0	0.0454	0.0118	0.03	5.356×10^{-4}	1.362×10^{-3}
61	3.0	0.0564	0.0118	0.03	6.658×10^{-4}	1.693×10^{-3}
62	43.4	0.0116	0.0118	0.03	1.373×10^{-4}	3.490×10^{-4}
63	6.9	0.1099	0.0118	0.03	1.297×10^{-3}	3.298×10^{-3}
64	51.6	0.1099	0.0118	0.03	1.297×10^{-3}	3.298×10^{-3}
65	12.5	0.0112	0.0118	0.03	1.326×10^{-4}	3.370×10^{-4}
66	32.5	0.0005	0.0118	0.03	5.853×10^{-6}	1.488×10^{-5}
67	33.1	0.0454	0.0118	0.03	5.356×10^{-4}	1.362×10^{-3}
68	6.1	0.0006	0.0118	0.03	7.024×10^{-6}	1.786×10^{-5}
69	43.2	0.0858	0.0118	0.03	1.012×10^{-3}	2.574×10^{-3}
70	7.3	0.0895	0.0118	0.03	1.056×10^{-3}	2.684×10^{-3}
71	95.5	0.0858	0.0118	0.03	1.012×10^{-3}	2.574×10^{-3}
72	15.9	0.0454	0.0118	0.03	5.356×10^{-4}	1.362×10^{-3}
73	5.0	0.0858	0.0118	0.03	1.012×10^{-3}	2.574×10^{-3}
74	3.4	0.0895	0.0118	0.03	1.056×10^{-3}	2.684×10^{-3}
75	18.3	0.0116	0.0118	0.03	1.373×10^{-4}	3.490×10^{-4}
76	64.9	0.0449	0.0118	0.03	5.297×10^{-4}	1.347×10^{-3}
77	18.9	0.0454	0.0118	0.03	5.356×10^{-4}	1.362×10^{-3}
78	7.6	0.0564	0.0118	0.03	6.658×10^{-4}	1.693×10^{-3}
79	26.8	0.0895	0.0118	0.03	1.056×10^{-3}	2.684×10^{-3}
80	4.8	0.0454	0.0118	0.03	5.356×10^{-4}	1.362×10^{-3}

81	116.6	0.0858	0.0118	0.03	1.012×10^{-3}	2.574×10^{-3}
82	9.3	0.0564	0.0118	0.03	6.658×10^{-4}	1.693×10^{-3}
83	87.7	0.1099	0.0118	0.03	1.297×10^{-3}	3.298×10^{-3}
84	74.8	0.0115	0.0118	0.03	1.355×10^{-4}	3.445×10^{-4}
85	50.8	0.0449	0.0118	0.03	5.297×10^{-4}	1.347×10^{-3}
86	59.5	0.0449	0.0118	0.03	5.297×10^{-4}	1.347×10^{-3}
87	24.5	0.1099	0.0118	0.03	1.297×10^{-3}	3.298×10^{-3}
88	21.6	0.1099	0.0118	0.03	1.297×10^{-3}	3.298×10^{-3}
89	5.7	0.0564	0.0118	0.03	6.658×10^{-4}	1.693×10^{-3}
90	5.4	0.0564	0.0118	0.03	6.658×10^{-4}	1.693×10^{-3}
91	11.1	0.0564	0.0118	0.03	6.658×10^{-4}	1.693×10^{-3}
92	15.2	0.0454	0.0118	0.03	5.356×10^{-4}	1.362×10^{-3}
93	42.1	0.0858	0.0118	0.03	1.012×10^{-3}	2.574×10^{-3}
94	52.5	0.0895	0.0118	0.03	1.056×10^{-3}	2.684×10^{-3}
95	2.0	0.0115	0.0118	0.03	1.355×10^{-4}	3.445×10^{-4}
96	8.9	0.0901	0.0118	0.03	1.063×10^{-3}	2.702×10^{-3}
97	2.0	0.1099	0.0118	0.01	1.297×10^{-3}	1.099×10^{-3}
98	56.3	0.0901	0.0118	0.03	1.063×10^{-3}	2.702×10^{-3}
99	15.8	0.1099	0.0118	0.03	1.297×10^{-3}	3.298×10^{-3}
100	39.9	0.1099	0.0118	0.03	1.297×10^{-3}	3.298×10^{-3}